Journal of Applied Mathematics and Physics, 2023, 11, 2545-2567
https://www.scirp.org/journal/jamp
ISSN Online: 2327-4379
ISSN Print: 2327-4352

# Unsteady Hydromagnetic Non-Newtonian Nanofluid Flow Past a Porous Stretching Sheet in the Presence of Variable Magnetic Field and Chemical Reaction

**Kafunda Tuesday[1*], Mathew N. Kinyanjui[2], Kang'ethe Giterere[2]**

[1]Department of Mathematics, Pan African University Institute of Basic Sciences, Technology and Innovation, Juja, Kenya
[2]Department of Pure and Applied Mathematics, Jomo Kenyatta University of Agriculture and Technology, Juja, Kenya
Email: *kafunda.tuesday@jkuat.ac.ke

**How to cite this paper:** Tuesday, K., Kinyanjui, M.N. and Giterere, K. (2023) Unsteady Hydromagnetic Non-Newtonian Nanofluid Flow Past a Porous Stretching Sheet in the Presence of Variable Magnetic Field and Chemical Reaction. *Journal of Applied Mathematics and Physics*, **11**, 2545-2567.
https://doi.org/10.4236/jamp.2023.119165

**Received:** August 14, 2023
**Accepted:** September 10, 2023
**Published:** September 13, 2023



## Abstract

The aim of this study is to examine the unsteady hydromagnetic flow of non-Newtonian nanofluid past a stretching sheet in the presence of variable magnetic field and chemical reaction. The system of non-linear partial differential equations governing the flow was solved using finite difference numerical approximation method. The resulting numerical schemes were simulated in MATLAB software. Furthermore, the skin-friction coefficient, Sherwood number, and Nusselt number have been presented in tabular form and discussed. The findings demonstrated that increasing Reynolds number increases velocity profiles while increasing permeability parameter, suction parameter and angle of inclination for the applied magnetic field reduces the velocity profiles of the fluid flow. Temperature of the fluid increases as the angle of inclination, magnetic number, Reynolds number and Eckert number increase but decreases as Prandtl number increases. Induced magnetic field profiles decrease as magnetic Prandtl number and suction parameter increase. Concentration profiles decrease as the chemical reaction parameter and Schmidt number increase but increase as the Soret number increases. The study is significant because fluid flow and heat transfer mechanisms with the variable magnetic considerations play an important role in magnetohydrodynamic generator or dynamo and magnetohydrodynamic pumps, nuclear reactors, vehicle thermal control, heat exchangers, cancer therapy, wound treatment and hyperthermia.

## Keywords

Hydromagnetic, Non-Newtonian, Nanofluid, Porous, Variable Magnetic Field, Chemical Reaction

## 1. Introduction

In recent years, numerous researchers have conducted in-depth studies on the hydromagnetic fluid flows past stretching sheets. The study of hydromagnetic nanofluid flows has attracted reasonable attention to fluid dynamics researchers since nanofluids possess enhanced heat transfer and energy efficiency characteristics that make them suitable for a wide range of engineering applications in various thermal systems.

[1] investigated laminar, boundary layer, MHD hybrid nanofluid flow and heat transfer driven by mixed convection adjacent to a vertical porous plate in the existence of magnetic induction was accounted for. The study aimed to investigate the effects of nonlinear thermal radiations on energy transport, particularly considering the influences of conduction-radiation and magnetic Prandtl number. The results showed that the induced magnetic field decreased as the Hartmann and magnetic Reynolds numbers increased.

[2] investigated numerical and statistical approaches to capture the flow characteristics of Maxwell hybrid nanofluid containing copper and graphene nanoparticles. The aim of this study was to analyze the properties of a hybrid nanofluid consisting of electrically conducting copper and graphene nanoparticles as it flows past a linearly stretched sheet, where there is a velocity slip condition at the interface. The results showed that Maxwell parameter, velocity slip and porosity had a tendency to reduce the hybrid nanofluid velocity whereas graphene Maxwell hybrid nanofluids temperature is getting enhanced for rising the values of magnetic fields inclination angle, radiation, unsteadiness parameters, Biot number and viscous dissipation.

Hydromagnetics refers to the study of the flow of electrically conducting fluids in the presence of magnetic fields. Examples of such fluids include electrolytes, plasma and liquid metals [3]. [4] studied heat transfer of magnetohydrodynamic stratified dusty fluid flow through an inclined irregular porous channel. The density and viscosity of the working fluid were assumed to vary along with the height of the channel as it behaves as a replica of many real world mechanisms. The results showed that an increase in the stratification decay parameter resulted in a stronger fluid flow momentum, and that the temperature was higher in the convective boundary compared to the Navier slip boundary.

[5] investigated the effect of two-dimensional Darcy-Forchheimer flow over second-grade fluid with linear stretching. Heat transfer through convective boundary conditions is taken into account. Results showed that temperature distribution rises by Dufour number whereas concentration distribution rises by Soret number. The Forchheimer number and porosity parameter raise the skin friction coefficient. The use of nanofluids in heat exchangers can potentially reduce both volumetric and mass flow rates, thereby leading to an overall decrease in power consumption as investigated in the works of [6].

[7] studied analysis of chemically reactive hydromagnetic Maxwell fluid conveying tiny particles due to Navier partial slip. The results showed that Navier

slip parameter increases as the velocity distribution decreases, while it enhances both the temperature and concentration distributions, increase in the radiation parameter enhances the temperature distribution, and the chemical reaction increment leads to decrease in concentration distribution.

[8] analyzed the impact of Hall current and induced magnetic field on the free convective flow of an electrically conducting, viscous, and incompressible fluid between two non-conducting vertical walls. The findings showed that the increase in Hall current resulted in an increase in both components of velocity, while both components of the induced magnetic field and induced current density decreased [9].

[10] investigated MHD fluid flow due to an unsteady stretching sheet with thermal radiation, porous medium and variable heat flux. According to their findings, the presence of a magnetic field is necessary to achieve efficient heat transfer, which is essential in many applications. Additionally, a high conductivity parameter leads to a significant rise in temperature adjacent to the sheet.

The present study is an extension of the recent work of [10] by incorporating variable magnetic field, variable coefficient of dynamic viscosity, unsteadiness, variable thermal conductivity, inclined applied magnetic field, magnetic induction, effects of chemical reaction and Soret effects, Lorentz force, Joule heating, effects of viscous dissipation, rates of heat and mass transfer and skin-friction coefficient.

Nanofluids are useful in a wide range of technical applications, including plasma physics, magnetic drug aiming, astronomy and astrophysics, and in electric power generation systems with high efficiency and low emissions [11]. [12] conducted a study on the magneto-hydrodynamics (MHD) boundary layer (BL) heat and mass transfer flow of thermally radiating and dissipative fluid over an infinite plate of vertical orientation with the involvement of induced magnetic field and thermal diffusion. The findings revealed that an increase in the suction parameter leads to a reduction in the values of velocity, temperature, and concentration.

[13] investigated the impacts of nanoparticle shape on $Al_2O_3$-water nanofluid flow and heat transfer over a non-linear radically stretching sheet. It was demonstrated that lamina shape nanoparticles had showed large temperature distribution than other shapes of nanoparticles.

In addition, the induced magnetic decreased as the magnetic parameter increased.

[14] investigated heat transfer on hydromagnetic Casson fluid flow in a porous medium influenced by thermal radiation. The results indicated that enlargement in magnetic number and permeability parameter showed decline in velocity profile but an opposite trend for temperature.

Numerous studies have been conducted on hydromagnetic fluid flows with various factors taken into consideration as illustrated above, however, not much attention has been given to the unsteady hydrodynamic flow of nanofluids past a stretching sheet in the presence of variable magnetic field and chemical reaction.

## 2. Mathematical Formulation

Consider the two dimensional and incompressible unsteady hydomagnetic non-Newtonian nanofluid flow past a porous stretching sheet in the presence of variable magnetic field and chemical reaction. The applied magnetic field is given by $\boldsymbol{B}_0 \cos\alpha \boldsymbol{i} + \boldsymbol{B}_0 \sin\alpha \boldsymbol{j}$ where $\alpha$ is the angle of inclination and the total magnetic field is $\boldsymbol{B} = \left(\boldsymbol{B}_0 \cos\alpha + \boldsymbol{B}_x\right)\boldsymbol{i} + \left(\boldsymbol{B}_0 \sin\alpha + \boldsymbol{B}_y\right)\boldsymbol{j}$ where $\boldsymbol{B}_x$ and $\boldsymbol{B}_y$ represent the induced magnetic field components along $x$ and $y$ directions respectively.

The fluid is being injected or sucked at different times with constant velocity $v = v_0$ where $v_0 > 0$ represents constant injection velocity while $v_0 < 0$ represents constant suction velocity. At time $t \le 0$, the velocity of the nanofluid is zero since the flow is surface driven so beyond the boundary layer, the fluid possesses back the velocity before getting in contact with the stretching plate, its temperature $T = T_\infty$, its concentration $C = C_\infty$, induced magnetic fields $\boldsymbol{H}_x = \boldsymbol{H}_y = 0$. For the no-slip boundary condition to be satisfied, when $t > 0$ and $y = 0$, the velocity of the nanofluid along $x$ direction $u = U_\infty$, the temperature of the nanofluid $T = T_{ss}$, its concentration $C = C_{ss}$ and magnetic induction $\boldsymbol{H}_x = \boldsymbol{H}_y = \boldsymbol{H}_0$ because the fluid tries to resist the changes caused by the applied magnetic field. As the distance $y \to \infty$ for $t > 0$, the velocity of the nanofluid along $x$ direction is zero, its temperature $T = T_\infty$, its concentration $C = C_\infty$, induced magnetic fields $\boldsymbol{H}_x = \boldsymbol{H}_y = 0$ (Figure 1).

## 3. Governing Equations

**Continuity equation**

Considering the velocity $v = v_0$ along $y$-direction as constant velocity, then the continuity equation becomes

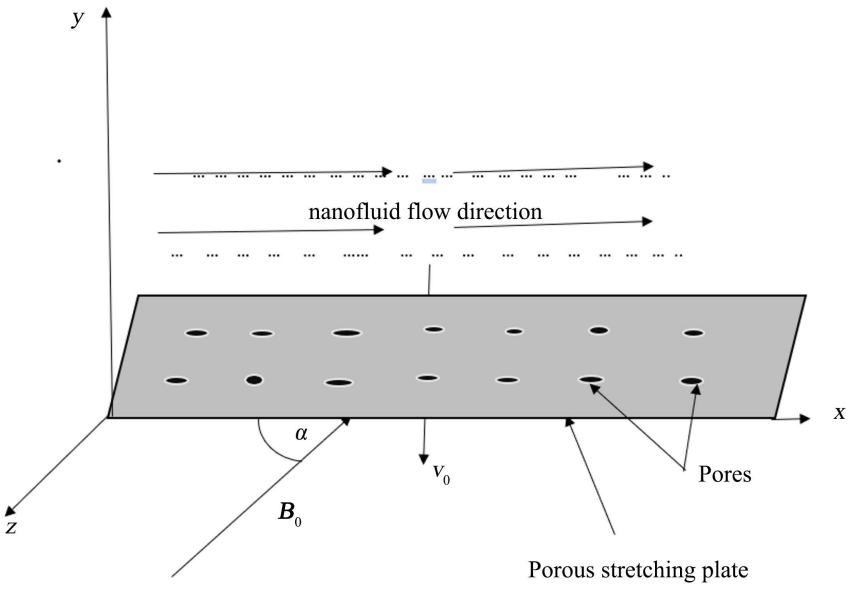


**Figure 1.** Physical diagram of the problem.

$$\frac{\partial u}{\partial x}=0 \tag{1}$$

Therefore, velocity and other variables in this study are considered to be functions of space coordinate $y$ and time $t$ only.

Equation of momentum along $x$ direction

$$\begin{aligned}\frac{\partial u}{\partial t}+v_0\frac{\partial u}{\partial y}&=\frac{\mu_\infty}{\rho_{n_f}\left(1+\delta\left(T-T_\infty\right)\right)}\left(\frac{u}{K}+\frac{\partial^2 u}{\partial y^2}\right)\\&\quad-\sigma\mu_e^2\left[u\left(\boldsymbol{H}_0\sin\alpha+\boldsymbol{H}_y\right)-v_0\left(\boldsymbol{H}_0\cos\alpha+\boldsymbol{H}_x\right)\right]\left(\boldsymbol{H}_0\sin\alpha+\boldsymbol{H}_y\right)\end{aligned} \tag{2a}$$

Equation of momentum along $y$ direction

$$\begin{aligned}&\frac{\partial v_0}{\partial t}+u\frac{\partial v_0}{\partial x}+v_0\frac{\partial v_0}{\partial y}\\&=\frac{\mu_\infty}{\rho_{n_f}\left(1+\delta\left(T-T_\infty\right)\right)}\left(\frac{v_0}{K}+\frac{\partial^2 v_0}{\partial x^2}+\frac{\partial^2 v_0}{\partial y^2}\right)\\&\quad+\sigma\mu_e^2\left[u\left(\boldsymbol{H}_0\sin\alpha+\boldsymbol{H}_y\right)-v_0\left(\boldsymbol{H}_0\cos\alpha+\boldsymbol{H}_x\right)\right]\left(\boldsymbol{H}_0\cos\alpha+\boldsymbol{H}_x\right)\end{aligned} \tag{2b}$$

Simplifying (2b)

$$\begin{aligned}&\sigma\mu_e^2\left[u\left(\boldsymbol{H}_0\sin\alpha+\boldsymbol{H}_y\right)-v_0\left(\boldsymbol{H}_0\cos\alpha+\boldsymbol{H}_x\right)\right]\left(\boldsymbol{H}_0\cos\alpha+\boldsymbol{H}_x\right)\\&=-\frac{\mu_\infty}{\rho_{nf_f}\left(1+\delta\left(T-T_\infty\right)\right)}\left(\frac{v_0}{K}\right)\end{aligned} \tag{2c}$$

Substituting (2c) in (2a), momentum equation becomes

$$\frac{\partial u}{\partial t}+v_0\frac{\partial u}{\partial y}=\frac{\mu_\infty}{\rho_{n_f}\left(1+\delta\left(T-T_\infty\right)\right)}\left(\frac{u}{K}+\frac{\partial^2 u}{\partial y^2}+\frac{v_0\left(\boldsymbol{H}_0\sin\alpha+\boldsymbol{H}_y\right)}{K\left(\boldsymbol{H}_0\cos\alpha+\boldsymbol{H}_x\right)}\right) \tag{3}$$

Energy equation

$$\begin{aligned}\frac{\partial T}{\partial t}+v_0\frac{\partial T}{\partial y}&=\frac{k_\infty}{\rho_{n_f}c_p}\left[1+\varepsilon\left(\frac{T-T_\infty}{T_{ss}-T_\infty}\right)\right]\left(\frac{\partial^2 T}{\partial y^2}\right)+\frac{\mu_\infty}{\rho_{n_f}c_p\left(1+\delta\left(T-T_\infty\right)\right)}\left(\frac{\partial u}{\partial y}\right)^2\\&\quad+\frac{\sigma\mu_e^2\left[u\left(\boldsymbol{H}_0\sin\alpha+\boldsymbol{H}_y\right)-v_0\left(\boldsymbol{H}_0\cos\alpha+\boldsymbol{H}_x\right)\right]^2}{\rho_{n_f}c_p}\end{aligned} \tag{4}$$

Magnetic induction equation along $x$ direction

$$\frac{\partial \boldsymbol{H}_x}{\partial t}=\boldsymbol{H}_0\sin\alpha\frac{\partial u}{\partial y}+\frac{\partial u\boldsymbol{H}_y}{\partial y}-v_0\frac{\partial \boldsymbol{H}_x}{\partial y}+\frac{1}{\mu_e\sigma}\left(\frac{\partial^2 \boldsymbol{H}_x}{\partial y^2}\right) \tag{5}$$

Magnetic induction equation along $y$ direction

$$\frac{\partial \boldsymbol{H}_y}{\partial t}=\frac{1}{\mu_e\sigma}\left(\frac{\partial^2 \boldsymbol{H}_y}{\partial y^2}\right). \tag{6}$$

Concentration equation

$$\frac{\partial C}{\partial t}=D_m\left(\frac{\partial^2 C}{\partial y^2}\right)-v_0\frac{\partial C}{\partial y}+\frac{D_m K_t}{T_m}\frac{\partial^2 T}{\partial y^2}-k_r\left(C-C_\infty\right). \tag{7}$$

The corresponding initial and boundary conditions are as follows:

$$t \le 0 : u = 0, T = T_\infty, C = C_\infty, H_x = H_y = 0, 0 \le y < \infty$$

$$t > 0 : \begin{cases} u = U_\infty, T = T_{ss}, C = C_{ss}, H_x = H_y = H_0 & y = 0 \\ u = 0, T = T_\infty, C = C_\infty, H_x = H_y = 0 & y \to \infty \end{cases} \tag{8}$$

The following dimensionless quantities were used to non-dimensionalize the governing equations for the present hydromagnetic flow problem, where $h$ is the length of the stretching plate

$$H_x = H_x^* H_0, H_y = H_y^* H_0, x = hx^*, y = hy^*,$$

$$t = \frac{h^2 t^*}{\nu_{n_f}}, u = U_\infty u^*, T = T_\infty + \left(T_{ss} - T_\infty\right) T^*, C = C_\infty + \left(C_{ss} - C_\infty\right) C^* \tag{9}$$

Using the above dimensionless variables, the governing equations in non-dimensional form are as follows:

Momentum equation

$$\frac{\partial u^*}{\partial t^*} = -Re \cdot S \cdot \frac{\partial u^*}{\partial y^*} + X \cdot u^* + \frac{\partial^2 u^*}{\partial y^{*2}} + X \cdot S \cdot \frac{\sin\alpha + H_y^*}{\cos\alpha + H_x^*} \tag{10}$$

Energy equation

$$\begin{aligned} \frac{\partial T^*}{\partial t^*} = -Re \cdot S \frac{\partial T^*}{\partial y^*} + \frac{1}{P_r}\left(\frac{\partial^2 T^*}{\partial y^{*2}}\right) + E_c \left(\frac{\partial u^*}{\partial y^*}\right)^2 \\ + M \cdot E_c \left[\left(\sin\alpha + H_y^*\right) - S \cdot \left(\cos\alpha + H_x^*\right)\right]^2 \end{aligned} \tag{11}$$

Magnetic induction equation along $x$ direction

$$\frac{\partial H_x^*}{\partial t^*} = Re\left(\sin\alpha \frac{\partial u^*}{\partial y^*} + u^* \frac{\partial H_y^*}{\partial y^*} + H_y^* \frac{\partial u^*}{\partial y^*}\right) - Re \cdot S \frac{\partial H_x^*}{\partial y^*} + \frac{1}{P_{r_m}}\left(\frac{\partial^2 H_x^*}{\partial y^{*2}}\right) \tag{12}$$

Magnetic induction equation along $y$ direction

$$\frac{\partial H_y^*}{\partial t^*} = \frac{1}{P_{r_m}}\left(\frac{\partial^2 H_y^*}{\partial y^{*2}}\right) \tag{13}$$

Concentration equation

$$\frac{\partial C^*}{\partial t^*} = \frac{1}{S_c}\left(\frac{\partial^2 C^*}{\partial y^{*2}}\right) - Re \cdot S \cdot \frac{\partial C^*}{\partial y^*} + S_r \frac{\partial^2 T^*}{\partial y^{*2}} - \gamma C^* \tag{14}$$

The corresponding initial and boundary conditions are as follows:

$$t^* \le 0 : u^* = 0, T^* = 0, C^* = 0, H_x^* = H_y^* = 0, 0 \le y^* < \infty$$

$$t^* > 0 : \begin{cases} u^* = 1, T^* = 1, C^* = 1, H_x^* = H_y^* = 1 & y^* = 0 \\ u^* = 0, T^* = 0, C^* = 0, H_x^* = H_y^* = 0 & y^* \to \infty \end{cases} \tag{15}$$

## 4. Numerical Solution

The governing Equations (10) - (14) are non-linear partial differential equations, therefore cannot be solved analytically. The numerical solutions for velocity,

temperature, magnetic induction and concentration profiles are solved using finite difference method subject to the initial and boundary conditions (15). The space and time intervals are fixed at $\Delta y = 0.02$ and $\Delta t = 0.00001$ respectively to ensure stability and convergence of the numerical solution. Equations (10) - (14) at the grid point $(j,k)$ are expressed in difference form, where the spatial partial derivatives are approximated using central difference approximations and temporal partial derivatives are approximated using forward difference approximation as follows :

$$u_j^{k+1} = u_j^k - Re\cdot S\cdot \Delta t\frac{u_{j+1}^k - u_{j-1}^k}{2\Delta y} + X\cdot u_j^k\cdot \Delta t + \frac{u_{j+1}^k - 2u_j^k + u_{j-1}^k}{(\Delta y)^2} + X\cdot S\cdot \Delta t\left(\frac{\sin\alpha + H_{y_j}^k}{\cos\alpha + H_{x_j}^k}\right)$$

$$T_j^{k+1} = T_j^k - Re\cdot S\cdot \Delta t\left(\frac{T_{j+1}^k - T_{j-1}^k}{2\Delta y}\right) + P_r\cdot \Delta t\left(\frac{T_{j+1}^k - 2T_j^k + T_{j-1}^k}{(\Delta y)^2}\right) + E_c\cdot \Delta t\left(\frac{u_{j+1}^k - u_{j-1}^k}{2\Delta y}\right)^2 + M\cdot E_c\cdot \Delta t\left[\left(\sin\alpha + H_{y_j}^k\right) - S\cdot\left(\cos\alpha + H_{x_j}^k\right)\right]^2$$

$$H_{x_j}^{k+1} = H_{x_j}^k + Re\cdot \Delta t\left(\sin\alpha\left(\frac{u_{j+1}^k - u_{j-1}^k}{2\Delta y}\right) + u_j^k\left(\frac{H_{y_{j+1}}^k - H_{y_{j-1}}^k}{2\Delta y}\right) + H_{y_j}^k\left(\frac{u_{j+1}^k - u_{j-1}^k}{2\Delta y}\right)\right) - Re\cdot S\cdot \Delta t\left(\frac{H_{y_{j+1}}^k - H_{y_{j-1}}^k}{2\Delta y}\right) + \frac{\Delta t}{P_{r_m}}\left(\frac{H_{x_{j+1}}^k - 2H_{x_j}^k + H_{x_{j-1}}^k}{(\Delta y)^2}\right) \tag{16}$$

$$H_{y_j}^{k+1} = H_{y_j}^k + \frac{\Delta t}{P_{r_m}}\left(\frac{H_{y_{j+1}}^k - 2H_{y_j}^k + H_{y_{j-1}}^k}{(\Delta y)^2}\right)$$

$$C_j^{k+1} = C_j^k + \frac{\Delta t}{S_c}\left(\frac{C_{j+1}^k - 2C_j^k + C_{j-1}^k}{(\Delta y)^2}\right) - Re\cdot S\cdot \Delta t\left(\frac{C_{j+1}^k - C_{j-1}^k}{2\Delta x}\right) + S_r\cdot \Delta t\left(\frac{T_{j+1}^k - 2T_j^k + T_{j-1}^k}{(\Delta y)^2}\right) - \gamma C^*\cdot \Delta t$$

Subject to the following initial and boundary conditions

$$t \le 0 : u(j,0) = 0, T(j,0) = 0, C(j,0) = 0, H_x(j,0) = H_y(j,0) = 0, 0 \le y < \infty$$

$$t > 0 : \begin{cases} u(0,k) = 1, T(0,k) = 1, C(0,k) = 1, H_x(0,k) = H_y(0,k) = 1 & y = 0 \\ u(j,k) = 0, T(j,k) = 0, C(j,k) = 0, H_x(j,k) = H_y(j,k) = 0 & y \to \infty \end{cases} \tag{17}$$

Skin-friction coefficient, Sherwood number and Nusselt number are defined as follows:

$$Nu = \frac{y' T_y}{T_{ss} - T_\infty}$$

$$C_f = \frac{h\tau}{\rho_{nf} U_\infty \nu_{n_f}} \tag{18}$$

$$Sh = \frac{y'C_y}{C_{ss} - C_\infty}$$

where

$$T_y = -\left(\frac{\partial T}{\partial y}\right)_{y=0} = -\left(\frac{T_{ss} - T_\infty}{h}\right)\left(\frac{\partial T^*}{\partial y^*}\right)_{y^*=0},$$

$$\tau = \mu_{nf}\left(\frac{\partial u}{\partial y}\right)_{y=0} = \mu_{nf}\left(\frac{U_\infty}{h}\right)\left(\frac{\partial u^*}{\partial y^*}\right)_{y^*=0}$$

where

$$\mu_{nf} = \frac{\mu_\infty}{1+\delta\left(T - T_\infty\right)} \quad \text{and} \quad C_y = -\left(\frac{\partial C}{\partial y}\right)_{y=0} = -\left(\frac{C_{ss} - C_\infty}{h}\right)\left(\frac{\partial C^*}{\partial y^*}\right)_{y^*=0}.$$

Substituting these in (18) to obtain

$$Nu \cdot Re_y^{-1} = -\left(\frac{\partial T^*}{\partial y^*}\right)_{y^*=0}, C_f = \left(\frac{\partial u^*}{\partial y^*}\right)_{y^*=0}, Sh \cdot Re_y^{-1} = -\left(\frac{\partial C^*}{\partial y^*}\right)_{y^*=0} \tag{19}$$

Expressing Nusselt number, Skin Friction coefficient and Sherwood number in finite difference form using forward difference approximations.

$$\begin{aligned} Nu \cdot Re_y^{-1} &= -\left(\frac{T_{j+1}^k - T_j^k}{\Delta y}\right)_{y=0} \\ C_f &= \left(\frac{u_{j+1}^k - u_j^k}{\Delta y}\right)_{y=0} \\ Sh \cdot Re_y^{-1} &= -\left(\frac{C_{j+1}^k - C_j^k}{\Delta y}\right)_{y=0} \end{aligned} \tag{20}$$

## 5. Results and Discussion

To investigate the physical significance of the flow problem, the effects of various dimensionless parameters on the flow variables have been represented graphically and discussed while the skin-friction coefficient, Sherwood number and Nusselt number have been presented in tabular form and discussed. The numerical solutions have been evaluated by fixing the values of various dimensionless parameters involved in the problem such as $Re = 1$, $Pr = 0.71$, $S = 1$, $M = 1$, $P_{r_m} = 0.01$, $X = 2$, $Ec = 0.03$, $\alpha = \frac{\pi}{9}$, $Sc = 0.22$, $Sr = 0.2$ and $\gamma = 1$.

From Figure 2, it is observed that increase in the Reynolds number (*Re*) leads to an increase in the velocity profiles. Increasing Reynolds number means reduction in the viscous forces in the fluid and in turn the fluid particles tend to move at a higher velocity since they are experiencing less resistance.

From Figure 3, it is evident that higher values of the permeability parameter (*X*) lead to a reduction in the velocity profiles. An increase in the permeability

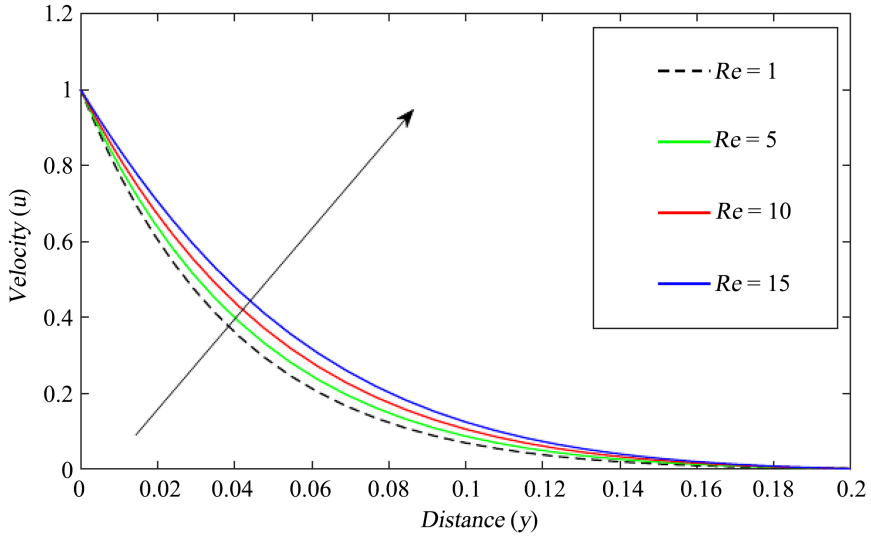


**Figure 2.** Velocity profiles for different values of *Re*.

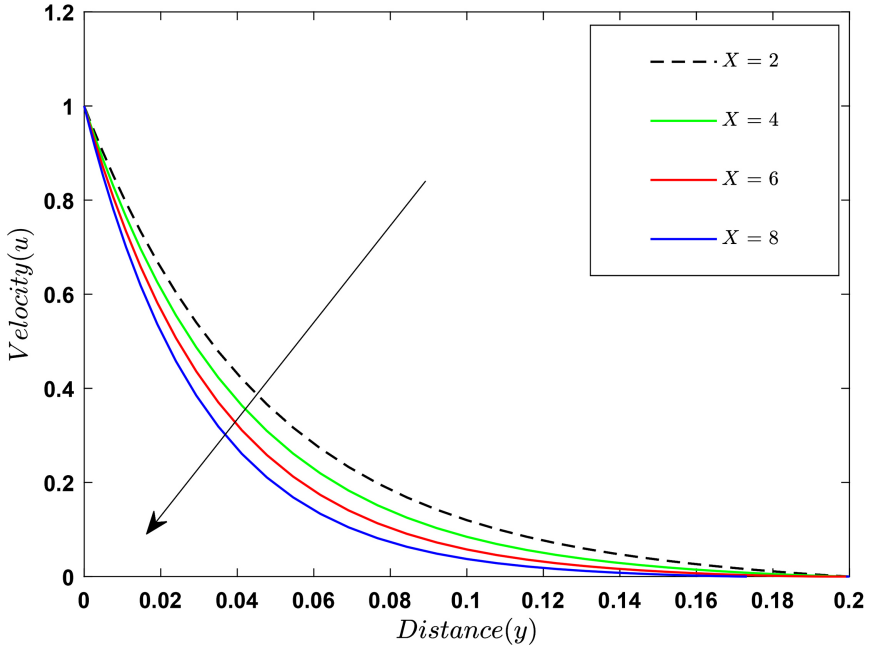


**Figure 3.** Velocity profiles for different values of *X*.

parameter indicates a greater porosity of the stretching sheet, which, in turn, reduces the acceleration of the fluid flow. Consequently, the increased permeability causes more resistance to the fluid motion, resulting in a thinner velocity boundary layer and ultimately leading to a decrease in the fluid velocity.

From **Figure 4**, it is observed that increasing suction parameter leads to a decrease in the velocity of the fluid when ($S > 0$) but increasing injection parameter ($S < 0$) increases fluid velocity profiles. ($S < 0$) means that fluid particles are being removed from the flow system and this tends to draw fluid particles in the vertical direction which leads to reduction in the flow's velocity in the x-direction

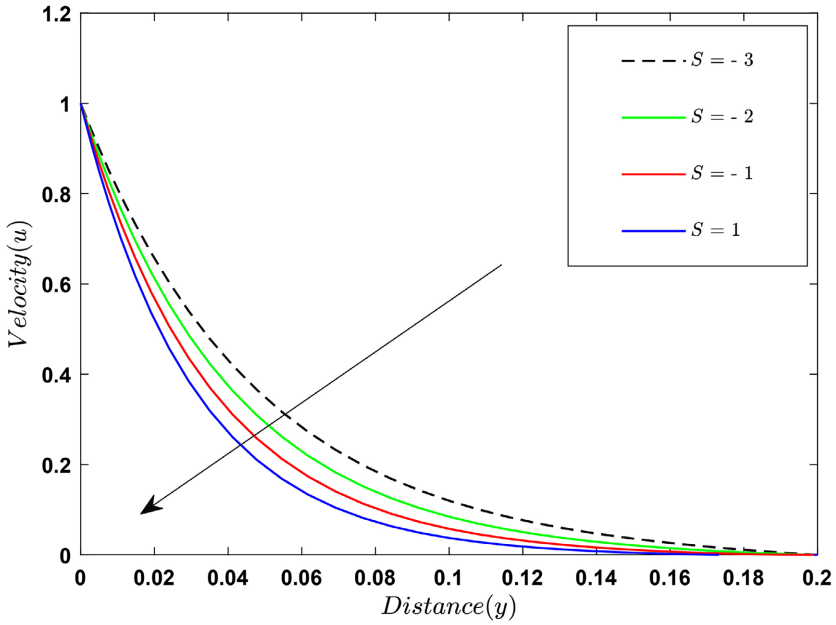


**Figure 4.** Velocity profiles against varying values of *S*.

because some of the fluid's kinetic energy is diverted into the vertical direction. However, when ($S > 0$), it implies introducing additional fluid particles into the fluid flow system, leading to a rise in the flow's velocity in the x-direction because an increased number of fluid particles now contribute to the overall flow.

From **Figure 5**, it is observed that increasing the angle of inclination for the applied magnetic field reduces velocity of the fluid. This is because increasing the angle of inclination enhances the applied magnetic field. Generally, an increase in the magnetic field generates the opposite force to the flow, called Lorentz force. This force has a tendency of reducing the velocity of the fluid.

From **Figure 6**, it is observed that increasing Eckert number increases the temperature of the nanofluid. Since Eckert number is the ratio of kinetic energy to enthalpy of the nanofluid flow, an increase in the Eckert number indicates that the kinetic energy energy of the fluid dominates over its enthalpy and the fluid experiences convective heating as the kinetic energy of the fluid is converted into thermal energy as it flows past a stretching plate. This thermal energy is produced in form of internal energy or heat and in turn the temperature of the fluid increases.

From **Figure 7**, it is observed that increase in the magnetic number leads to an increase in the temperature of the fluid. Since magnetic number is the ratio of magnetic forces to fluid inertia forces, so an increase in the magnetic parameter implies an increase in the magnetic forces and less inertia forces. So if the fluid particles in motion interact with higher magnetic field strength, this leads to induced electric current and the fluid particles collide with the charged particles of the current, this causes vibrations and produces thermal energy in form of heat. Therefore, increasing magnetic number leads to an increase in the temperature of the fluid.

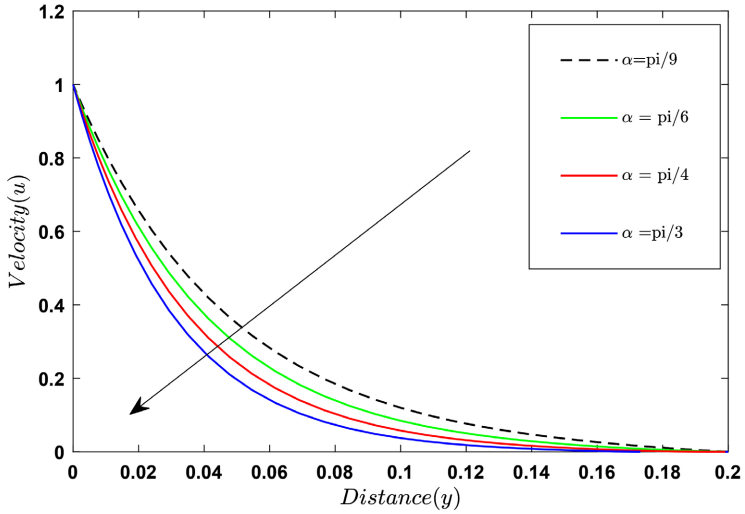


**Figure 5.** Velocity profiles for different values of *a*.

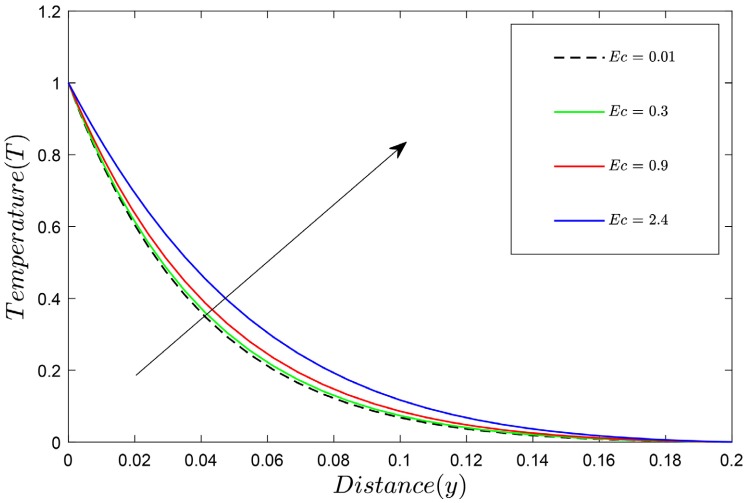


**Figure 6.** Temperature profiles for different values of *Ec*.

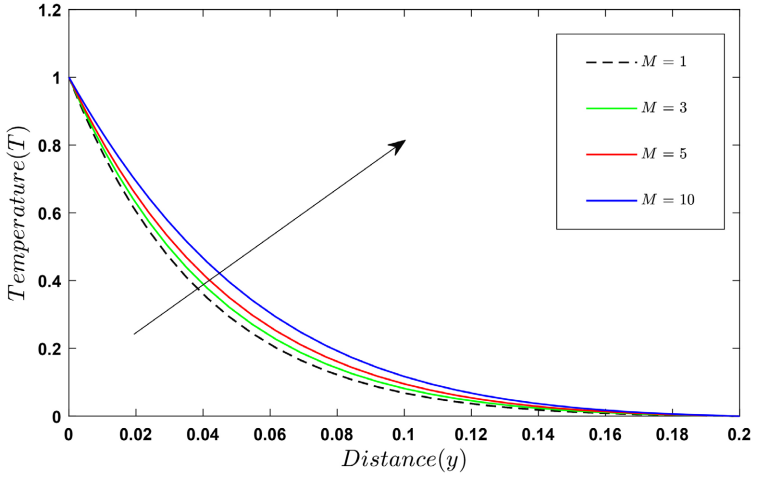


**Figure 7.** Temperature profiles for different values of *M*.

From Figure 8, it is observed that increasing Reynolds number leads to an increase in the temperature profiles. Since Reynolds number is the ratio of inertia forces to viscous forces, so increasing Reynolds number implies that the viscous forces become less significant. A decrease in viscous forces means that fluid particles have increased motion and heat is generated due to collision of the particles which are moving at high velocity thereby increasing fluid temperature.

Figure 9 shows the effects of Prandtl number on temperature profiles. The physical significance of changing the Prandtl number lies in its effect on the heat transfer characteristics of a fluid since it affects how heat is transferred within the fluid and from the fluid to surrounding surfaces. It is observed that increasing the Prandtl number leads to a decrease in the temperature of the fluid. Prandtl number is the ratio of momentum diffusivity to thermal diffusivity. Increasing the Prandtl number reduces the thermal diffusivity and increase viscosity of the fluid which leads to decrease in thermal boundary layer and thus results in decrease in the temperature of the fluid.

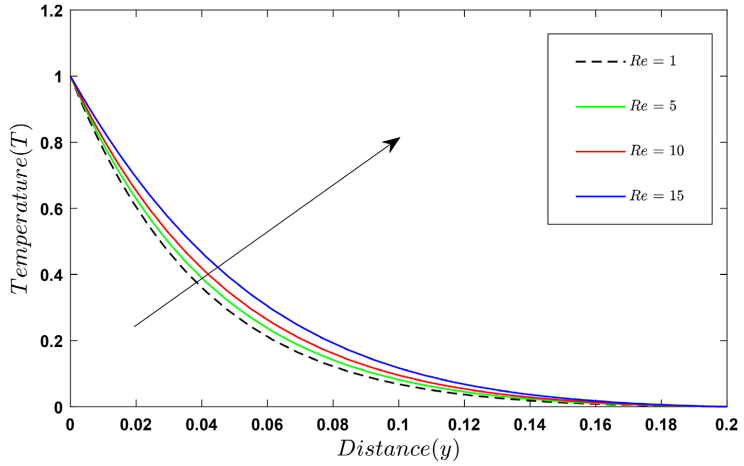


Figure 8. Temperature profiles for different values of *Re*.

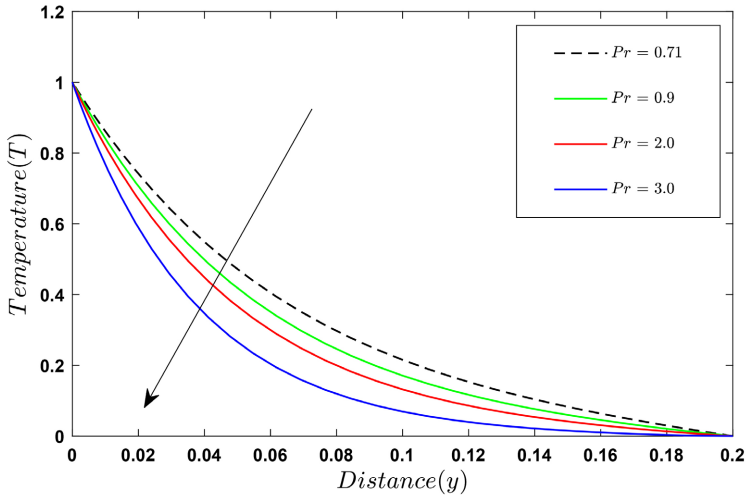


Figure 9. Temperature profiles for different values of *Pr*.

From Figure 10, it is observed that increasing magnetic Prandtl number leads to a decrease in induced magnetic field long x direction. When the magnetic Prandtl number, which represents the ratio of momentum diffusivity to magnetic diffusivity, increases, it indicates a decrease in magnetic diffusivity. Consequently, the induced magnetic field generated by the motion of the conducting medium decreases, resulting in a reduction of induced magnetic profiles along the x-direction.

From Figure 11, it is observed that increase in the Reynolds number leads to an increase in the induced magnetic field profiles along x direction. Since Reynolds number is the ratio of inertia forces to the viscous forces, so increasing Reynolds number implies reduction in the viscous forces which leads to an increase in the interaction between the fluid and the magnetic field and thus leading to an increase in the induced magnetic field.

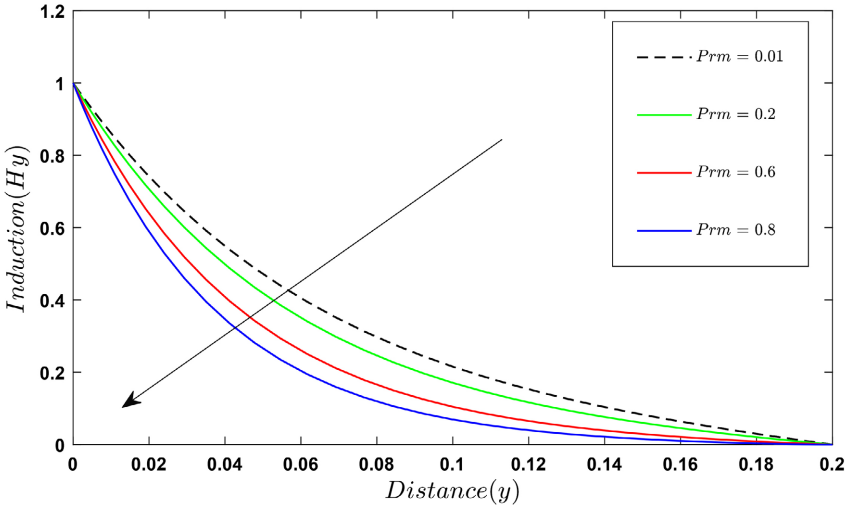


**Figure 10.** Induced magnetic profiles ($H_x$) for different values of $Pr_m$.

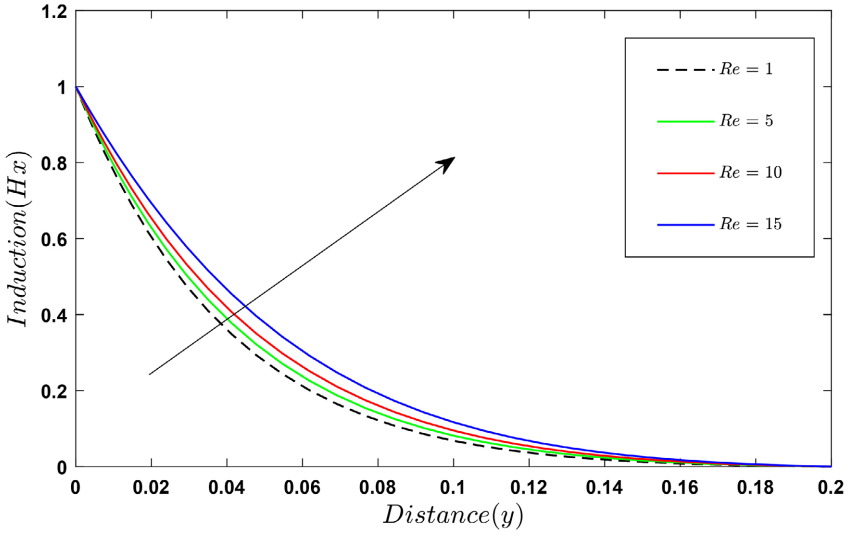


**Figure 11.** Induced magnetic profiles ($H_x$) for different values of $Re$.

From Figure 12, it is observed that increasing the suction/injection parameter reduces induced magnetic field profiles. Since suction parameter is the ratio of the suction velocity to the uniform velocity of the stretching sheet, so increasing this parameter reduces the velocity of the stretching sheet and since this flow is surface driven it implies that the velocity of the fluid decreases. This reduces the interaction between the fluid and the magnetic field and thus leading to decrease in the induced magnetic field profiles.

From Figure 13, it is observed that increasing magnetic Prandtl number leads to a decrease in induced magnetic field profiles. Since magnetic Prandtl number is the ratio of momentum diffusivity to the magnetic diffusivity, so increasing magnetic Prandtl number implies reduction in magnetic diffusion rate is low as the viscosity diffusion rate becomes stronger and this which leads to decrease in the induced magnetic field profiles.

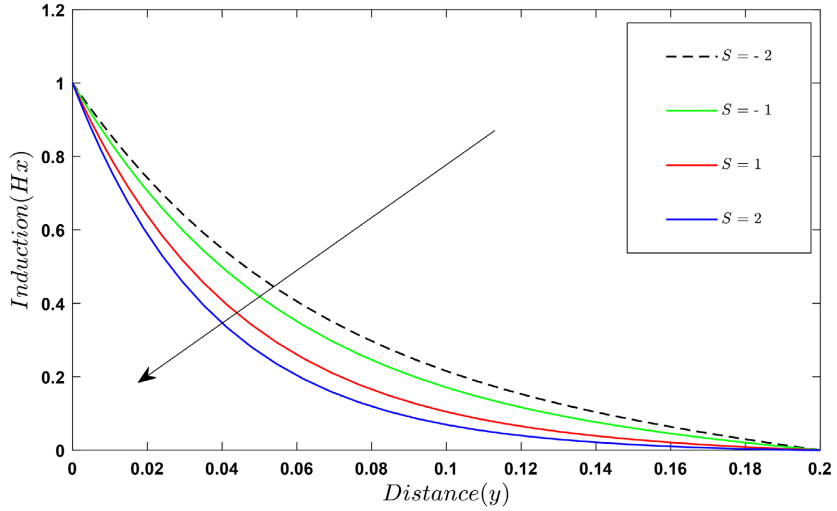


**Figure 12.** Induced magnetic profiles ($H_x$) for different values of $S$.

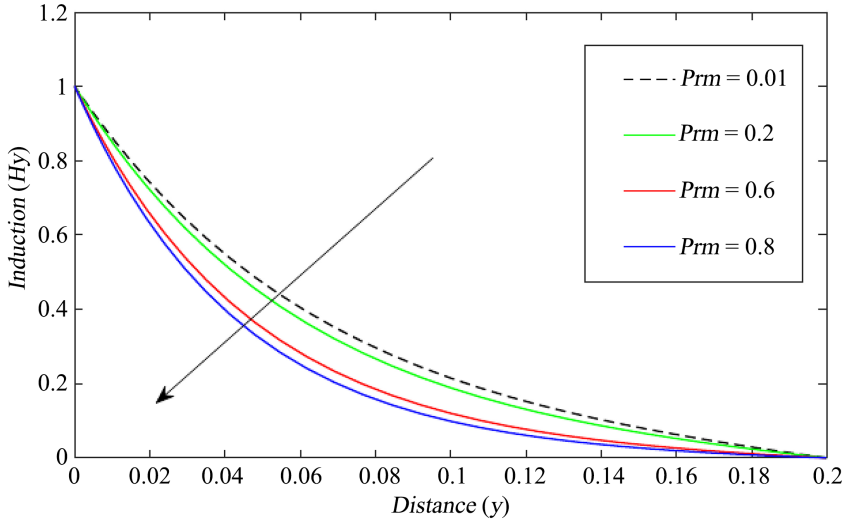


**Figure 13.** Induced magnetic profiles ($H_y$) for different values of $Pr_m$.

From Figure 14, it is observed that the concentration of the nanofluid decreases as the Schmidt number increases. Since Schmidt number is the ratio of momentum diffusivity to mass diffusivity of particles, increasing this parameter implies reduction in mass diffusivity and this leads to decrease in the concentration profiles of the nanofluid.

From Figure 15, it is observed that increasing Soret number increases concentration profiles. The Soret number determines the effect of the temperature gradients inducing significant mass diffusion effects. Increasing Soret number generates mass flux that leads to an increase in the mass boundary layer thickness. Therefore, an increase in the Soret number results to an increase in the concentration of the fluid.

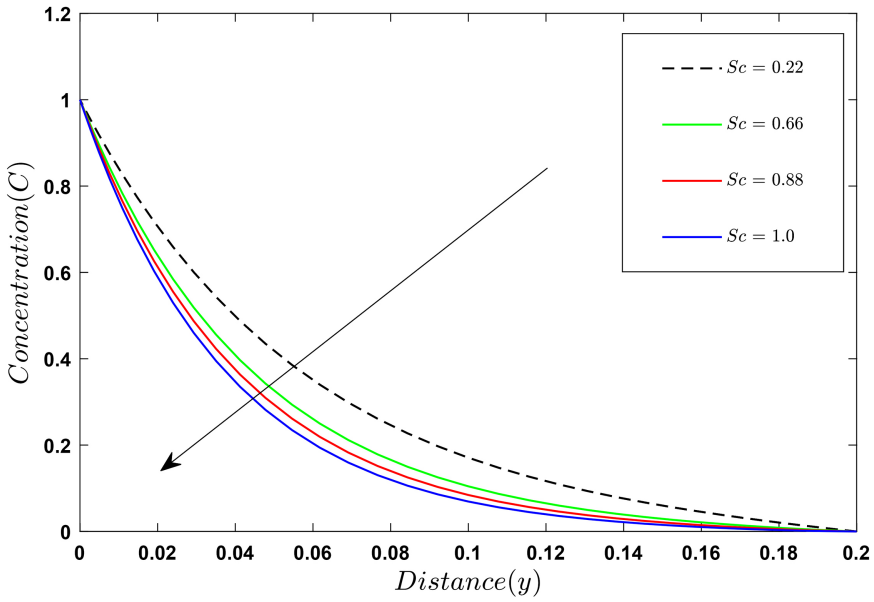


Figure 14. Concentration profiles ($C$) for different values of $Sc$.

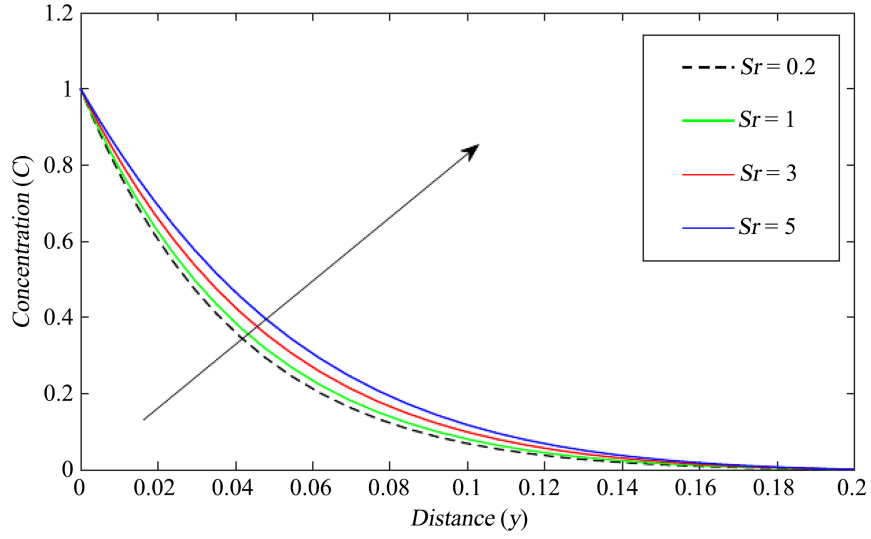


Figure 15. Concentration profiles ($C$) for different values of Soret number.

From Figure 16, it is observed that increase in the chemical reaction parameter leads to a decrease in the concentration of the fluid particles. A higher chemical reaction parameter indicates that the chemical reaction proceeds at a faster rate relative to the fluid transport. As a result, more reactants are consumed or converted into products in a given time, leading to a decrease in the concentration of the reactants in the fluid. In a chemical reaction, the reactant species decrease in concentration as they undergo chemical changes to form the products. As the chemical reaction progresses, the reactant molecules collide and react, leading to the formation of products. As a result, the concentration of the reacting species decreases because the molecules are being converted into new products and this leads to a decrease in the chemical molecular diffusivity.

Table 1 shows that as Reynolds number increases, the skin-friction coefficient reduces in magnitude. This is because as Reynolds number increases, the coefficient of dynamic viscosity reduces and since the skin friction coefficient is directly proportional to the coefficient of dynamic viscosity, then the skin-friction also reduces. At low Reynolds numbers, the viscous forces dominate over the inertia forces. The flow is smooth and ordered, with fluid particles moving in well-defined layers. The skin friction coefficient, which measures the frictional drag of the fluid on a solid surface, tends to be relatively higher because of the strong interaction between the fluid and the solid surface. The shear stress between fluid layers is significant, resulting in a higher skin friction coefficient. Additionally, increasing the values of permeability parameter, suction/injection parameter and angle of inclination for the applied magnetic field decreases the skin-friction coefficient in magnitude.

Table 2 shows that increasing Schmidt number reduces Sherwood number while increasing Soret number and chemical reaction parameter increases Sherwood number. The chemical reaction parameter enhances mass transfer by generating

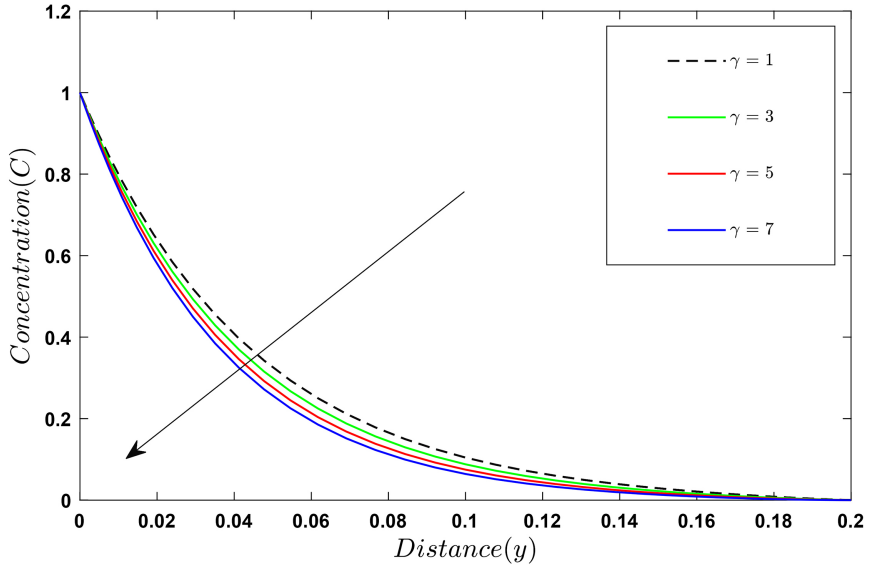


Figure 16. Concentration profiles ($C$) for different values of $\gamma$.

**Table 1.** Results of Skin-friction coefficient for various physical parameters.

| $Re$ | $X$ | $S$ | $a$ | $-Cf$ |
|---|---|---|---|---|
| 1 | 2 | 1 | $\frac{\pi}{9}$ | 4.22051 |
| 5 | 2 | 1 | $\frac{\pi}{9}$ | 2.63383 |
| 10 | 2 | 1 | $\frac{\pi}{9}$ | 1.32005 |
| 15 | 2 | 1 | $\frac{\pi}{9}$ | 0.57334 |
| | 4 | 1 | $\frac{\pi}{9}$ | 3.96262 |
| | 6 | 1 | $\frac{\pi}{9}$ | 3.70168 |
| | 8 | 1 | $\frac{\pi}{9}$ | 3.43761 |
| | | 2 | $\frac{\pi}{9}$ | 3.65790 |
| | | 3 | $\frac{\pi}{9}$ | 3.13618 |
| | | 4 | $\frac{\pi}{9}$ | 2.65460 |
| | | | $\frac{\pi}{6}$ | 4.19410 |
| | | | $\frac{\pi}{4}$ | 4.14642 |
| | | | $\frac{\pi}{3}$ | 4.08241 |

**Table 2.** Results of Sherwood number for various physical parameters.

| $Sc$ | $Sr$ | $\gamma$ | $Shw$ |
|---|---|---|---|
| 0.22 | 0.2 | 1 | −4.9051 |
| 0.66 | 0.2 | 1 | −4.73928 |
| 0.88 | 0.2 | 1 | −4.65858 |
| 1.0 | 0.2 | 1 | −4.61562 |
| | 1 | 1 | −4.97794 |
| | 3 | 1 | −5.14903 |
| | 5 | 1 | −5.32011 |
| | | 3 | −4.93877 |
| | | 5 | −4.96797 |
| | | 7 | −4.99710 |

concentration gradients through rapid chemical reactions, while the Soret number enhances mass transfer by inducing concentration gradients due to thermal diffusion effects.

Table 3 shows that increasing the values of the angle of inclination, Eckert number and magnetic number increases the Nusselt number by facilitating an increase in convective heat transfer due to the increased kinetic energy of the flow. However, increasing the values of suction/injection parameter and Prandtl number reduces the Nusselt number. This is because increasing the angle of inclination, Eckert number and magnetic number increases rate of heat transfer thereby increasing thermal boundary layer thickness while increasing suction/injection parameter and Prandtl number leads to thinning of the thermal boundary layer thickness. Increasing Nusselt number signifies the presence of convective heat transfer at the boundary in the fluid whereas decreasing Nusselt number signifies conductive heat transfer at the boundary is dominant.

## 6. Validation of Results

In validating the numerical code for the accuracy of the computed results, the

Table 3. Results of nusselt number for various physical parameters.

| $a$ | $S$ | $Pr$ | $Ec$ | $M$ | $Nu$ |
|---|---|---|---|---|---|
| $\frac{\pi}{9}$ | 1 | 0.71 | 0.01 | 1 | −4.60415 |
| $\frac{\pi}{6}$ | 1 | 0.71 | 0.01 | 1 | −4.60437 |
| $\frac{\pi}{4}$ | 1 | 0.71 | 0.01 | 1 | −4.60457 |
| $\frac{\pi}{3}$ | 1 | 0.71 | 0.01 | 1 | −4.60463 |
| | 2 | 0.71 | 0.01 | 1 | −4.27284 |
| | 3 | 0.71 | 0.01 | 1 | −3.95466 |
| | 4 | 0.71 | 0.01 | 1 | −3.64966 |
| | | 0.9 | 0.01 | 1 | −4.50465 |
| | | 2 | 0.01 | 1 | −3.96632 |
| | | 3 | 0.01 | 1 | −3.52033 |
| | | | 0.3 | 1 | −4.14100 |
| | | | 0.9 | 1 | −4.24345 |
| | | | 2.4 | 1 | −4.54232 |
| | | | | 3 | −4.60365 |
| | | | | 5 | −4.60373 |
| | | | | 10 | −4.60192 |

present results for the effects of permeability parameter and Prandtl number on Nusselt number are compared with the results obtained by [5] who investigated Dufour and Soret effects on Darcy-Forchheimer flow of second grade fluid with the variable magnetic field and thermal conductivity.

| $K$ | $Pr$ | Khan *et al.* [5] | Present study |
|---|---|---|---|
| 0.3 | 1 | 0.19498 | 0.19488 |
| 0.5 | 1 | 0.19496 | 0.19479 |
| 0.7 | 1 | 0.19495 | 0.19467 |
| 0.2 | 1.1 | 0.19402 | 0.19400 |
| 0.2 | 1.2 | 0.19302 | 0.19301 |
| 0.2 | 1.3 | 0.19209 | 0.19202 |

It can be observed that the results are in high agreement.

## 7. Concluding Remarks

In this study, the problem of the unsteady hydromagnetic flow of non-Newtonian nanofluid past a stretching sheet in the presence of variable magnetic field and chemical reaction has been examined. The system of the governing equations in PDE form was solved using finite difference method. The numerical results for the velocity, temperature, induced magnetic fields and concentration profiles are presented graphically for the pertinent parameters. The numerical values for skin-friction coefficient, Sherwood and Nusselt numbers are presented in tabular form.

## Acknowledgements

The authors express their gratitude to the Pan African University Institute of Basic Science, Technology and Innovation (PAUISTI) for their timely support throughout the conduct of the research. Gratitude also goes to Jomo Kenyatta University of Agriculture Science and Technology (JKUAT) for hosting PAUISTI. Appreciation goes to the African Union through PAUISTI for sponsoring the research study.

## Data Availability

The data used to support the findings is available with the researcher, can be shared if needed.

## Conflicts of Interest

The authors declare they have no conflicts of interest.

## References

[1] Alharbi, S.O. (2021) Impact of Hybrid Nanoparticles on Transport Mechanism in

Magnetohydrodynamic Fluid Flow Exposed to Induced Magnetic Field. *Ain Shams Engineering Journal*, **12**, 995-1000. https://doi.org/10.1016/j.asej.2020.04.013

[2] Bhattacharyya, A., Sharma, R., Hussain, S., Chamkha, A. and Mamatha, E. (2022) A Numerical and Statistical Approach to Capture the Flow Characteristics of Maxwell Hybrid Nanofluid Containing Copper and Graphene Nanoparticles. *Chinese Journal of Physics*, **77**, 1278-1290. https://doi.org/10.1016/j.cjph.2021.09.015

[3] Hazarika, G. and Phukan, B. (2017) Effects of Variable Viscosity and Thermal Conductivity on Steady Magnetohydrodynamic Flow of a Micropolar Fluid through a Specially Characterized Horizontal Channel. *Modelling Measurement and Control B*, **86**, 1-13.

[4] Kalpana, G. and Saleem, S. (2022) Heat Transfer of Magnetohydrodynamic Stratified Dusty Fluid Flow through an Inclined Irregular Porous Channel. *Nanomaterials*, **12**, Article No. 3309. https://doi.org/10.3390/nano12193309

[5] Khan, A.A., Naeem, S., Ellahi, R., Sait, S.M. and Vafai, K. (2020) Dufour and Soret Effects on Darcy-Forchheimer Flow of Second-Grade Fluid with the Variable Magnetic Field and Thermal Conductivity. *International Journal of Numerical Methods for Heat & Fluid Flow*, **30**, 4331-4347. https://doi.org/10.1108/HFF-11-2019-0837

[6] Kinyanjui, M. and Onyango, E.R. (2022) Hydromagnetic Surface Driven Flow between Two Parallel Vertical Plates in the Presence of Chemical Reaction and Induced Magnetic Field. *Global Journal of Pure and Applied Mathematics*, **18**, 583-612.

[7] Koriko, O.K., Oladipupo, V.A., Omowaye, A.J. and Oni, S.T. (2021) Analysis of Chemically Reactive Hydromagnetic Maxwell Fluid Conveying Tiny Particles Due to Navier Partial Slip. *Open Access Library Journal*, **8**, 1-18. https://doi.org/10.4236/oalib.1108003

[8] Kumar, D., Singh, A. and Kumar, D. (2018) Effect of Hall Current on the Magnetohydrodynamic Free Convective Flow between Vertical Walls with Induced Magnetic Field. *The European Physical Journal Plus*, **133**, Article No. 207. https://doi.org/10.1140/epjp/i2018-12012-4

[9] Masoud Hosseini, S., Safaei, M. R., Estell'e, P. and Hadi Jafarnia, S. (2020) Heat Transfer of Water-Based Carbon Nanotube Nanofluids in the Shell and Tube Cooling Heat Exchangers of the Gasoline Product of the Residue Fluid Catalytic Cracking Unit. *Journal of Thermal Analysis and Calorimetry*, **140**, 351-362. https://doi.org/10.1007/s10973-019-08813-5

[10] Megahed, A.M., Ghoneim, N.I., Reddy, M.G. and El-Khatib, M. (2021) Magnetohydrodynamic Fluid Flow Due to an Unsteady Stretching Sheet with Thermal Radiation, Porous Medium, and Variable Heat Flux. *Advances in Astronomy*, **2021**, Article ID: 6686883. https://doi.org/10.1155/2021/6686883

[11] Mwamba, N., Okelo Abonyo, J., Awuor, K.O., *et al.* (2023) Effects of Thermal Radiation and Chemical Reaction on Hydromagnetic Fluid Flow in a Cylindrical Collapsible Tube with an Obstacle. *International Journal of Mathematics and Mathematical Sciences*, **2023**, Article ID: 9991376. https://doi.org/10.1155/2023/9991376

[12] Poddar, S., Islam, M.M., Ferdouse, J., Alam, M., *et al.* (2021) Characteristical Analysis of MHD Heat and Mass Transfer Dissipative and Radiating Fluid Flow with Magnetic Field Induction and Suction. *SN Applied Sciences*, **3**, Article No. 470. https://doi.org/10.1007/s42452-021-04452-4

[13] Rashid, U. and Ibrahim, A. (2020) Impacts of Nanoparticle Shape on $Al_2O_3$-Water Nanofluid Flow and Heat Transfer over a Non-Linear Radically Stretching Sheet. *Advances in Nanoparticles*, **9**, 23-39. https://doi.org/10.4236/anp.2020.91002

[14] Reddy, K.V. and Reddy, G.V.R. (2022) Outlining the Impact of Melting on MHD Casson Fluid Flow Past a Stretching Sheet in a Porous Medium with Radiation. *Biointerface Research in Applied Chemistry*, **13**, Article No. 42. https://doi.org/10.33263/BRIAC131.042

## Nomenclature

| Symbol | Meaning |
|---|---|
| $\boldsymbol{q}$ | Velocity vector ($m\cdot s^{-1}$) |
| $\boldsymbol{B}$ | Magnetic flux ($Wb\cdot m^{-2}$) |
| $\boldsymbol{H}$ | Magnetic field intensity ($Wb\cdot m^{-2}$) |
| $\boldsymbol{E}$ | Electric field intensity (v) |
| $\boldsymbol{B}_0$ | Applied inclined magnetic field vector ($Wb\cdot m^{-2}$) |
| $\boldsymbol{J}$ | Current density ($A\cdot M^{-2}$) |
| $v_0$ | Suction/injection velocity ($m\cdot s^{-1}$) |
| $P$ | Pressure force ($N\cdot m^{-2}$) |
| $k_{nf}$ | Nanofluid thermal conductivity ($W\cdot m^{-1}\cdot K^{-1}$) |
| $F$ | Body forces (N) |
| $T$ | Temperature of the nanofluid (K) |
| $c_p$ | Specific heat capacity at constant pressure ($J\cdot kg^{-1}\cdot K^{-1}$) |
| $P$ | Pressure ($N\cdot m^{-2}$) |
| $C$ | Species concentration (mole/kg) |
| $E$ | Specific internal energy ($kg\cdot m^{-1}\cdot s^{-1}$) |
| $T_{ss}$ | Temperature of the nanofluid at the stretching sheet (K) |
| $C_{ss}$ | Concentration of the nanofluid at the stretching sheet (mole/kg) |
| $D_m$ | Mass diffusivity/chemical molecular diffusivity ($m^2\cdot s^{-1}$) |
| $u$ | Velocity component along x direction ($m\cdot s^{-1}$) |
| $\rho_{n_f}$ | Nanofluid density ($kg\cdot m^{-3}$) |
| $\sigma$ | Electrical conductivity ($S^{-1}\cdot m^{-1}$) |
| $\mu_{n_f}$ | Nanofluid coefficient of dynamic viscosity ($kg\cdot m^{-1}\cdot s^{-1}$) |
| $\mu_e$ | Magnetic permeability ($H\cdot m^{-1}$) |
| $\phi$ | Viscous dissipation function ($s^{-1}$) |
| $\nu_{n_f}$ | Kinematic viscosity ($m^2\cdot s^{-1}$) |
| $u^*$ | Non-dimensional velocity component along x direction |
| $H_x$ | Induced magnetic field along x direction ($Wb\cdot m^{-2}$) |
| $H_y$ | Induced magnetic field along y direction ($Wb\cdot m^{-2}$) |
| $K_t$ | Thermal diffusion ratio ($m^2\cdot s$) |
| $h$ | Characteristic length (m) |
| $H^*$ | Non-dimensional induced magnetic field |
| $U_\infty$ | Constant velocity of the stretching sheet ($m\cdot s^{-1}$) |
| $\Delta y, \Delta t$ | Distance and time intervals |
| $k_r$ | Chemical reaction coefficient |
| $X$ | Permeability parameter |
| $Ec$ | Eckert number |
| $M$ | Magnetic parameter |
| $\gamma$ | Chemical reaction parameter |
| $Sr$ | Soret number |
| $S$ | Suction/injection parameter |
| $P_{r_m}$ | Magnetic Prandtl number |

| | |
|---|---|
| $Pr$ | Prandtl number |
| $Sc$ | Schmidt number |
| $Re$ | Reynolds number |

## Abbreviations

| | |
|---|---|
| **MHD** | Magnetohyrodynamic |
| **PDE** | Partial Differential Equations |
| **FDM** | Finite Difference Method |
| **FTCS** | Forward Time, Centered Space |
| **MATLAB** | Matrix Laboratory |